Journal of Materials Chemistry B

Accepted Manuscript

ROYAL SOCIETY OF CHEMISTRY

www.rsc.org/materialsB

Journal Name

ARTICLE

Modulation of the structural properties of mesoporous silica nanoparticles to enhance the T1-weighted MR imaging capability

Received 00th January 20xx,
Accepted 00th January 20xx

DOI: 10.1039/x0xx00000x

www.rsc.org/

Didem Şen Karaman[a,b], Diti Desai[a], Jixi Zhang[b,c], Sina Tadayon[b], Gözde Unal[b], Jarmo Teuho[d], Jawad Sarfraz[b], Jan-Henrik Smått[b], Hongchen Gu[e], Tuomas Näreoja[f], Jessica M. Rosenholm[a,b]*

In this study, we have investigated the contrast enhancement of gadolinium (III) incorporated nanoparticle-based contrast agents (CA) by the modulation of the synthesis and structural parameters of the mesoporous silica nanoparticle (MSN) matrix. In the optimization process, the structure of the MSN matrix, post synthesis treatment protocols, as well as the source and incorporation routes of paramagnetic gadolinium centers were considered, with the aim to shorten the T_1 weighted relaxation time. After preliminary evaluation of the prepared MSNs as nanoparticulate T_1/positive contrast agents based on relaxivity, the structure of the MSN matrix was affirmed as the most decisive property to enhance the r_1 relaxivity value, alongside the incorporation route of paramagnetic Gd (III) centers. Based on these evaluations, the most promising Gd (III) incorporated MSN-based CA candidate was further evaluated for its cytocompatiblity and intensity enhancement by *in vitro* phantom MR-imaging of labeled cells. Furthermore, pre-labeled tumors grown on a chick embryo chorioallantoic membrane (CAM) was imaged as an *in vivo* model on a 3T clinical MRI scanner. Our findings show that the optimized MSN-based CA design enables proper access of water to Gd-centers in the selected MSN matrices, and simultaneously decrease the required amount of Gd (III) content on a per-particle basis when evaluated against the other MSNs. Consequently, the required Gd amount on a per-dose basis is significantly decreased with regard to clinically used Gd-based CAs for T_1-weighted MR imaging.

Introduction

In clinical diagnosis, magnetic resonance imaging (MRI) has become one of the most powerful tools due to its spatial resolution and soft tissue contrast and penetration depth.[1] In MRI, contrast agents (CAs) are the most essential complementary tools which improve the sensitivity and detectability of this imaging technique. Contrast agents are classified as T_1-positive agents of paramagnetic species and T_2-negative agents of super-paramagnetic materials based on their relaxation processes. The majority of commercially available T_1 contrast agents are based on gadolinium (III) -containing molecular complexes, while the T_2 agents are iron oxide nanoparticles. The major advantage of T_1 contrast agents compared to T_2 contrast agents is the provided signal enhancement, which can maximize the strength of MRI by enhancing the contrast and visual detectability of pathological targets compared to non-malignant tissues. On the other hand, existing T_1 contrast agents have the drawbacks as molecular probes involving difficulties in tracking and not showing satisfactory contrast enhancement in the early stages of disease. On the contrary, the nanoparticulate features of T_2 imaging agents are very promising in this sense; however, still having the disadvantage of providing negative contrast that cause signal-decreasing effects, distortion and demolition in the anatomic backgrounds.[2] Therefore, novel contrast agents are needed to overcome disadvantages associated with the existing CAs by combining the beneficial characteristics of T_1 (clear distinctive signal enhancement) and T_2 (nanoparticulate feature) contrast agents.

In the literature, one of the first attempts in this direction was done by preparing a lipid-encapsulated liquid perfluorocarbon nanoparticle that carried Gd (III) complexes, thus creating a nanoscaled T_1 contrast agent platform.[3] Recently, several research studies have been carried out to devise T_1-nanoparticulate contrast agents by introducing various gadolinium (Gd) chelating agents based on diethylenetriaminepentaacetic acid (DTPA), diethylenetriaminetetraacetic acid (DTTA), n-(trimethoxysilylpropyl) ethyldiamine, triacetic acid trisodium salt (TSPETE) and 1,4,7,10-tetraazacyclododecane-1,4,7,10-tetraacetic acid (DOTA) to nanoparticulate carriers, such as

[a] Pharmaceutical Sciences Laboratory, Faculty of Science and Engineering, Åbo Akademi University, 20520 Turku, Finland.
[b] Laboratory of Physical Chemistry, Faculty of Science and Engineering, Åbo Akademi University, 20500 Turku, Finland.
[c] Key Laboratory of Biorheological Science and Technology, Ministry of Education, College of Bioengineering, Chongqing University, Chongqing 400044, China.
[d] Turku PET Centre, Turku University Hospital, 20521 Turku, Finland
[e] Nano Biomedical Research Center, School of Biomedical Engineering and Med-X Research Institute, Shanghai Jiao Tong University, Shanghai 200030, China
[f] . Laboratory of Biophysics, Faculty of Medicine, University of Turku, 20520 Turku, Finland

Electronic Supplementary Information (ESI) available: [details of any supplementary information available should be included here]. See DOI: 10.1039/x0xx00000x

high-density lipoproteins (HDL), non-porous/mesoporous silica nanoparticles and quantum dots.[4,5,6,7,8,9] In these studies, different approaches were employed to incorporate Gd-chelating agents on/in the nanoparticle matrices. Post-synthesis grafting and co-condensation during the synthesis of MSNs are two main approaches used in the literature, which also leads to distinct variations in the structural properties of the final particles.[10,11] Additionally, direct incorporation of Gd(III) ions into the nanoparticle's matrix has been carried out in order to provide one-step synthesis preparations.[12,13]

Recently, the structural properties of silica-based nanoparticles have emerged as a focus of investigation in order to, amongst others, vary their imaging capabilities. Importantly, the large surface areas, high pore volumes, tunable pore sizes and excellent biocompatibility of mesoporous silica particles provide an ideal platform to integrate diverse properties to the inside and/or outside surfaces of MSNs in a modular fashion.[14,15] When the imaging capabilities of mesoporus silica nanoparticles are considered among all the other properties, there exist various techniques to introduce detectability such as doping of organic dyes, co-condensation of fluorescent dyes and integration of metal crystals.[16]

During preparation of MSNs with imaging capabilities, the structural properties will have a significant influence on the gained characteristics. Already the mere formation of a mesoporous silica shell on core materials with MR-imaging capability has been established to result in remarkably increased relaxivity of the MRI-active core, due to diffusion of water molecules inside the pore channels.[17,18,19,20] When the MR-imaging capability is introduced using the MSN as a carrier for paramagnetic Gd (III), MSN has been considered as an ideal platform to evenly incorporate a large number of paramagnetic centers while still keeping them accessible to the surrounding water *via* the mesoporous channels.[21,22,23] For instance, it has been shown that alteration of the porous network in the mesoporous silica matrix leads to changes in the MR imaging capability. In the study of Guillet-Niclos et al.[24]MSN based contrast agents were prepared with 3D and 2D pore network architectures by introducing the Gd(III) ions in MSNs by the incipient wetness technique, in order to reach optimal 1H relaxation efficiency. According to their findings with the optimized concentration of Gd (III) ion incorporation, higher r_1 relaxivity values were obtained for the 3D network structured MSNs. The influence of the Gd chelating agent's localization on the relaxometric properties of MSNs was also explored by localizing the chelating agent either on the external surfaces of MSNs or inside the pores. It was found as the Gd (III) complexes are silent from a relaxometric point of view when they are localized inside the pore channels, where they are less accessible to water molecules than on the external surface of particles.[25] The effect of preparation-tuned Gd-DOTA location was also verified by co-condensing the chelating agents with the silica source during the synthesis step. Their so-called "long-delay co-condensation" preparative technique lead to a preferential distribution of chelating agents closer to the pore openings i.e. the particle surface.[26]

In view of this, while covalent conjugation of Gd-chelates has been reviewed as the most common approach for preparing MSN-based CAs for MRI in the literature,[10] this approach is also associated with certain drawbacks. First, the complexation of Gd to the chelates is a slow process for achieving the stable form of the complex.[27,28,29,30,31] Thus, the complexation can be carried out either before incorporation to the MSNs or the chelate can be incorporated to the MSNs by co-condensation or post-grafting before Gd complexation.[10,32,33] Besides the notion that complexation into a solid support-attached chelate presents itself with additional levels of complexity as compared to the complexation of molecular agents,[34] whereby the complexation for chelate-grafted solid silica nanoparticles has been reported to being conducted for up to 5 days in the literature;[35] similar time-scales are not applicable for MSN structures since long exposure times to aqueous media can lead to considerable structure deformation in MSN matrices.[36] Furthermore, the ample possibility of leaching of the chelates upon dissolution of the MSN matrix, is also likely during the Gd complexation process since this takes place under aqueous conditions.[37] Pre-complexing the Gd may, then again, induce hydrolysis of functional groups intended for further conjugation to MSNs. Due to these reasons, the confirmation of actual Gd complexation taking place in the abovementioned studies have been scarce, and when investigating the complexation process in more detail also non-specific binding of Gd has been found.[36] Further, it is clear from the above studies along with vast literature examples of functionalization with other active agents that these may preferentially accumulate on the particle surface/block the pore openings, in CA context to a degree that the chelates in the pores are not active from a relaxometric point of view due to restricted diffusion of water molecules.[24,25] This is not optimal neither from an imaging point of view, whereby the justification of using MSNs would be to utilize their large specific surface areas (not only the particle surface, whereby non-porous particles would work equally well) nor for systems with theranostic prospects, whereby considerably larger (such as drug) molecules than water would need to be accommodated in the pores. Consequently, we sought to evaluate the alternative approach i.e. direct doping of the silica matrix with paramagnetic Gd.

To expand the possibilities for guest molecule accommodation, recent breakthroughs in the field of developing novel designs for MSNs include the development of multi-functional hollow structured mesoporous silica particles.[38,39,40] Hollow mesoporous silica nanoparticles, that possess a large cavity inside each original mesoporous silica particle, can function as reservoirs for enhanced loading of guest (such as drug) molecules, and have thus gained a special interest within theranostic applications. The hollow structure has also shown to influence the MR imaging capability of inorganic particles, where significant enhancement in the r_1 relaxivity value of hollow-structured manganese oxide particles was observed as compared to solid manganese oxide nanoparticles.[41] Still, the reason of such a finding was left to the scope of further research, but lead us to believe that a hollow structure may

have an influence on doped matrices too. Thus, encouraged by the notion that Gd doping of silica matrices can provide an alternative way for introducing MR imaging capability to MSNs, we set out to address the effect of both structural and preparational parameters on the relaxometric properties of Gd doped MSNs. Thus, we conducted a systematic evaluation on the influence of commonly employed pre- and post-synthesis preparation routes together with commonly employed structural variations (e.g. hollow vs. regular) of MSNs on rationally enhancing their potential imaging capabilities. Consequently, we synthesized all-silica MSNs into which Gd (III) was introduced *via* different routes, while the structural features were modulated via different pre- and post-synthetic approaches. With the investigated designs, we have also aimed to still keep the mesoporous channels free to act as drug reservoirs for future therapeutic prospects, while maintaining a sufficient contrast enhancement capability.[42]

The series of prepared MSN-based CAs have been summarized in Scheme 1. The regular pore - sized mesoporous silica nanoparticle [MSN] and pore-expanded hollow-structured mesoporous silica nanoparticle [H-MSN] matrices were considered for their structural varieties to investigate the thus-provided longitudinal relaxivity (r_1) enhancement. In these preparations, Gd (III) paramagnetic centers are accumulated within the silica network, with the aid of which an efficient diffusion of water molecules throughout the MSN matrix and the interaction between the paramagnetic centers and neighboring water protons is ensured. Therefore, we envisioned that the prepared MSNs with larger pore sizes and hollow interiors would most likely have a mechanistic influence on the contrast enhancement, as compared to regular pore-sized MSNs. In addition, the incorporation strategies of Gd (III) paramagnetic centers *via* two different routes were investigated as a second parameter, whereby the introduction of two different types of gadolinium sources ($Gd(acac)_3$ and $GdCl_3$) into the matrices were performed by considering the variables of the MSN matrix. Two Gd-incorporation routes were carried out: by introducing Gd (III) sources directly in the synthesis step of MSNs (*in situ* synthesis) and after the MSNs had already been prepared (post synthesis). In the final step of the MSN-based CA preparation, the structure directing agent (SDA) removal procedure, solvent extraction and calcination, were investigated for their influence on the accommodation of Gd(III) into the MSN matrices.

Among the studied parameters, both the MSN structure and the doping routes of Gd(III) paramagnetic centers had a great impact on the performance of the MSNs as contrast agents with high longitudinal relaxivity (r_1). When the Gd (III) was doped into pore-expanded hollow-structured mesoporous silica nanoparticles (H-MSN) by employing *in situ* synthesis doping protocols, this resulted in almost 20-fold better r_1 relaxivity values as compared to the corresponding "regular" pore-sized MSN matrix. On the contrary, structure-dependent variation was not pronounced for the post synthesis doping preparations. Here, any differences were mainly observed between matrices within the same MSN structures which were prepared by solvent extraction and calcination SDA removal routes. More specifically, the calcined matrices resulted in almost 6-fold higher r_1 values as compared to solvent-extracted MSN matrices. As a result, the MSN-based contrast agent with the best potential from our optimization and screening analysis lowers the required concentration of Gd (III) to 30 μM with the r_1 value of 12.3 mM^{-1} s^{-1} as compared to the clinically used Magnevist® CA which is typically used in a concentration of 500 mM with a r_1 value of 3.6 mM-$1s^{-1}$.[43]

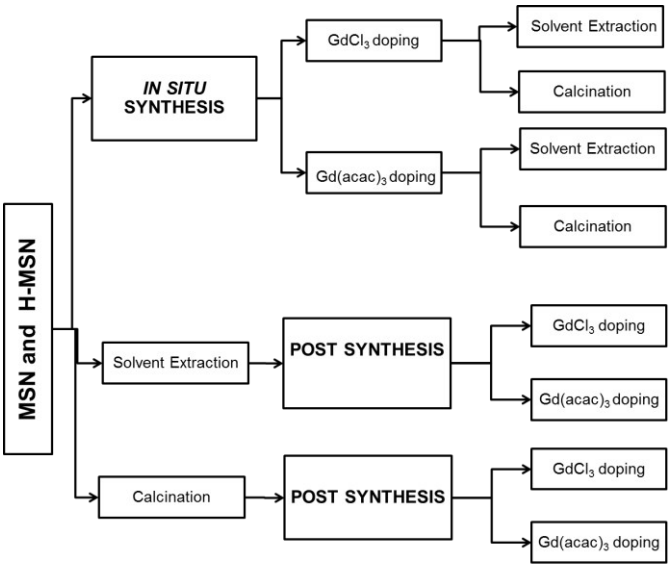

Scheme 1. Synthesis parameters of MSN based contrast agents

Experimental

Synthesis of MSN and H- MSN

Regular pore sized MSN were synthesized according to the protocol described in our previous study[44] with slight modifications, as follows: absolute ethanol was added to form an aqueous basic reaction solution of 20 v/v% concentration. Cetyltrimethylammonium bromide (CTAB), tetra ethylorthosilicate (TEOS) and aminopropyltriethoxysilane silane (APTES) were mixed into the basic aqueous reaction solution as structure-directing agent (SDA) and silica sources, respectively. The reaction was conducted in at 33 °C overnight. The molar composition of the final synthesis solution was 1 TEOS: 0.1 APTES: 0.12 CTAB: 0.32 NaOH: 73 EtOH: 946 H_2O. After overnight reaction, the MSNs were collected by centrifugation, washed with ethanol and separated into two batches in order to carry out two different routes of SDA removal: solvent extraction in ethanolic NH_4NO_3 solution and calcination at 550 °C overnight, respectively.

For the synthesis of pore-expanded hollow structured MSN [H-MSN] the protocol described in our previous study[45] was followed. Briefly, this was accomplished by increasing the structure directing agent (CTAB) content and adding the swelling agents decane and 1,3,5-trimethylbenzene (TMB) into

the MSN synthesis mentioned above. The molar composition of the final synthesis solution was 1 TEOS: 0.1 APTES: 0.85 decane: 0.18 CTAB: 0.55 TMB: 0.32 NaOH: 73 EtOH: 946 H_2O. The reaction was conducted at room temperature. Afterwards, the synthesis solution of H-MSN was hydrothermally treated *in situ* for two days at 70°C. As a last step of H-MSN matrix preparation, two different structure directing agent (SDA) removing routes were carried out, i.e. solvent extraction in ethanolic NH_4NO_3 solution and calcination. (The nomenclatures of all the prepared MSNsare available in the Supporting Information with explanations).

Gadolinium (III) ion incorporation strategies into MSN and H-MSN matrices

i. *In situ* synthesis doping of MSN matrices (Scheme 2a)

In this synthesis route, the Gd(III) sources $GdCl_3.6H_2O$ and Gd $(acac)_3.2H_2O$ were used. In the protocol water, ethanol and sodium hydroxide was mixed with the Gd(III) source ($GdCl_3.6H_2O$ and $Gd(acac)_3.2H_2O$) until completely dissolved. The stepwise addition of Gd(III) sources was continued up to the level of visual saturation which was 5 mol% and 3.5 mol% relative to the added silica source content, respectively. The same preparation method was also applied for the *in situ* doping of H-MSN matrices with the same concentrations. In order to decide the SDA removing route for the prepared *in situ* synthesis doped-MSNs, preliminary experiments were carried out by energy-dispersive X-ray spectroscopy technique for both calcined and solvent extracted *in situ* Gd (III) incorporated samples. According to the preliminary investigations, the most appropriate route to remove SDAs after *in situ* synthesis incorporation of Gd(III) ions was found to be the calcination process, which resulted in significantly higher amount of Gd(III) incorporation degree compared to the extraction process (approximately 2 w% Gd(III) incorporation for the calcined sample and 0.03 w% for the solvent extracted samples). Here, we may speculate that the calcination process may aid in "locking" the paramagnetic centers into the matrix, while solvent extraction may remove them by ion exchange during the extraction process. The produced samples from this part of the study are abbreviated $[MSN]_{cal.}$: $(GdCl_3)_{in\ situ}$, $[MSN]_{cal.}$: $(Gd(acac)_3)_{in\ situ}$ and $[H\text{-}MSN]_{cal.}$: $(GdCl_3)_{in\ situ}$, $[H\text{-}MSN]_{cal.}$: $(Gd(acac)_3)_{in\ situ}$ for *in situ* ($GdCl_3.6H_2O$) and Gd $(acac)_3.2H_20$ doped regular ([MSN]) and hollow structured ([H-MSN]) MSNs.

ii. *Post synthesis* doping of MSN matrices (Scheme2b)

First, pristine MSN and H-MSN matrices were prepared using the above-defined protocols, and the two different routes of SDS removal were carried out for the pristine MSNs; namley solvent extraction and calcination. Subsequently, the two different Gd(III) sources mentioned above ($GdCl_3.6H_2O$ and $Gd(acac)_3.2H_20$) were dissolved in HEPES buffer to the corresponding amounts (5 mol % and 3,5 mol % relative to the theoretical silicon amount per mass of sample that was used for *in situ* Gd(III) doping MSN and H-MSN procedures. For *post synthesis* doping preparations, the MSN suspensions and Gd(III) containing HEPES solutions were mixed and kept in a sonication bath for 30 minutes, after which the mixture was kept on a rotating wheel for 2.5h in order not to cause any distortion of the porous structure of MSNs by dissolution in aqueous media. As a final step of the p*ost synthesis* doping protocol, the samples were centrifuged and washed once, after which the obtained cake was dried under vacuum. The samples prepared by post synthesis doping method were abbreviated as $[MSN]_{cal.}$:$(GdCl_3)_{post}$, $[MSN]_{extr.}$:$(GdCl_3)_{post}$, $[MSN]_{cal.}$:$(Gd(acac)_3)_{post}$, $[MSN]_{extr.}$: $(Gd(acac)_3)_{post}$ and $[H\text{-}MSN]_{cal.}$: $(GdCl_3)_{post}$, $[H\text{-}MSN]_{extr.}$: $(GdCl_3)_{post}$, $[H\text{-}MSN]_{cal.}$: $(Gd(aca)_3)_{post}$, $[H\text{-}MSN]_{extr.}$: $(Gd(aca)_3)_{post}$ for $GdCl_3.6H_2O$ and $Gd(acac)_3.2H_2O$ for MSNs and H-MSNs for which the post-synthesis treatments solvent extraction (extr.) and calcination (cal.) were employed to remove the SDA.

Subsequently, the possible structural distortion during the complexation process of Gd (III) was determined by powder x-ray diffraction analysis and the accumulated Gd (III) amount in the prepared samples was analyzed by inductively-coupled plasma atomic emission spectrometry (ICP-AES).

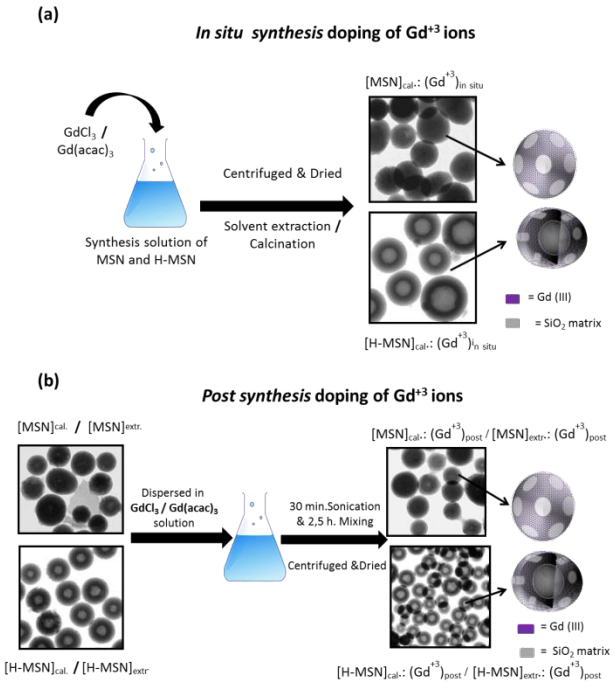

Scheme 2 Incorporation of gadolinium ions into MSN matrices by (a) *in situ* synthesis and (b) post synthesis methods.

Characterization of prepared MSNs and H-MSN

The morphological changes in the prepared MSN-based contrast agents were investigated by scanning electron microscopy imaging (LEO Gemini 1530, Leo Ltd, Oberkochen, Germany). The alterations in mesoscopic order of the materials were confirmed with powder x-ray diffraction analysis by using a Kratky compact small-angle system

M.Braun, Nottinghampshire, UK). Redispersibility and net surface charge of all prepared MSN and H-MSN-based contrast agents as well as the pristine MSNs were examined by redispersing the dried particles in HEPES buffer (25 mM at pH 7.2) with the help of ultra-sonication and subsequent dynamic light scattering (DLS) and zeta potential measurements (ZetaSizer NanoZS, Malvern,UK).

Inductively-coupled plasma atomic emission spectrometry (ICP-AES) was employed to determine the incorporated Gd (III) amount for the produced MSN-based contrast agents. The samples were pretreated by dissolving in hydrofluoric acid and diluted to the concentration 40 µg/mL before the measurements. After examining the amount of incorporated Gd (III) into the MSNs matrices , the T_1 and T_2 relaxation times per unit concentration of the sample were measured on a table-top NMR (MiniSpec) by using a 1.4 T Bruker Minispec Analyzer (MQ60). A total of 200 µL of each sample (diluted from stock suspension in water) were placed in a 10-mm sample tube and allowed to equilibrate at 37 °C in a circulating water bath. The most efficient MSN-based contrast agents were explored based on concentration of contrast agent vs T_1 relaxation time plot. Subsequently, the inverse of T_1 and T_2 value versus the gadolinium concentration (mM) plots for each sample were obtained, and the r_1 and r_2 values ($mM^{-1} s^{-1}$) were calculated by taking the slope of the curves.

X-ray photoelectron spectroscopy (XPS) and x-ray diffraction (XRD) measurements were carried out for the *in situ* and post synthesis doped MSNs in order to characterize the chemical composition of the incorporated Gd(III) into the silica network and investigate whether any recrystallization occurs during the doping. XPS spectra were obtained ~~with~~on a Physical Electronics Quantum 2000 scanning spectrometer using a monochromatic Al Kα X-ray source (1486.6 eV). The spectrometer pass energy was set to 58.7 eV and 187.85 eV for the detailed region and survey spectra, respectively. The atomic concentration (at. %) of the different elements was derived by calculating the area of the peaks and correcting for the sensitivity factors (using the software MultiPak v6.1A from Physical Electronics). XRD measurements were carried out on a Bruker AXS D8 Discover instrument (Karlsruhe, Germany) with a scintillation point detector using a Cu Kα X-ray source. The data was collected between 12–40° 2θ using a step size of 0.04° 2θ.

In vitro and *in vivo* studies

In the *in vitro* studies, the MSN-based contrast agent that displayed the best per-particle efficacy for the longitudinal proton relaxation time (T_1) and the highest r_1 relaxivity value was first evaluated for its cytocompatibility by the WST-1 assay to elucidate safe particle concentrations. Thereafter, this concentration was used to label human cervical cancer HeLa cells which were further used for phantom imaging and tumor formation on the Chick Embryo Chorioallantoic Membrane (CAM) as an *in vivo* model, in order to confirm the visualization of the labeled cells with magnetic resonance imaging (MRI).

Cell viability studies. HeLa (Human cervical adenocarcinoma) cells obtained from ATCC (Manassas, VA, USA) were maintained in DMEM medium (Sigma, St. Louis, MO, USA) supplemented with 10% fetal calf serum (BioClear, Wiltshire, UK), 2 mM L-glutamine, 100 U/ml penicillin, 100 µg/mL streptomycin at 37 °C in a 5% CO_2/95%O2 and 90 % RH humidify atmosphere and handled under sterile conditions. To investigate the effect of the particles on cell viability, HeLa cells were transferred to 96-well plates (6000 cells/well) and allowed to attach and grow. After 24 h, the medium was removed and replaced with 100 µL medium containing different concentrations of Gd(III) containing MSNs (10, 25, 50 µg/mL) for 48 h. After incubation, 10 µL of WST-1 reagent (Roche Applied Science, Upper Bavaria, Germany) was added to each well and the plate was further incubated for 90 min at 37°C in 5% CO_2. After incubation with WST-1 reagent, the absorbance of the colored formazan was measured at 430 nm wavelength using Varioskan microplate reader (Thermo Scientific, Logan UT, USA) to determine cell viability.

Cell labelling and phantom imaging. For magnetic resonance imaging (MRI), HeLa cells were incubated (in 100 mm diameter culture dishes) with the MSN-based contrast agents that preserved the structural properties of pristine H-MSN during the preparation and had the best *T*1 - contrast agent property at particle concentrations 0, 0.1, 1, 10 and 50 µg/mL at 37°C for 4 hours. After incubation, the culture media was removed and the cells were washed with phosphate buffered saline (PBS, pH 7.4) three times, trypsinized and washed once again with PBS. Cells were then transferred to 1.5 mL Eppendorf tubes at a concentration of $1.5*10^6$ cells/tube and pelleted. In the end, each Eppendorf tube was filled with 0.5 mL of 3% gelatin and then the samples were left to solidify before MRI measurements.

As further confirmation of contrast enhancement of the best MSN based T_1 contrast agent candidate, HeLa cells were incubated with the best potential MSN-based contrast agent at the concentration of 50 µg/mL and implanted on *in ova* Chick Embryo Chorioallantoic Membrane (CAM) as *in vivo* model with the detailed protocol presented in supplementary information file. CAM is an extraembryonic membrane, forms on the 4^{th} day incubation and HeLa cells which were labelled with the selected CA sample were implanted on the 8^{th} day to obtain tumors. The implanted tumors were labelled with the CA by following the protocols described in the supplementary information. As a final step, the tumors *in ova* were imaged on the 14^{th} day of incubation.

MR-Imaging was performed on a Philips Ingenuity TF 3.0 T PET/MRI scanner (Philips Healthcare, Cleveland, OH,USA). A dedicated small animal coil for preclinical imaging was used for MRI (8 ch Rat Whole-body Coil, Rapid Biomedical GmbH, Germany). The MR sequence parameters used for both phantom and CAM model imaging are given in the supplementary information.

The total signal intensities measured from the MR images of phantom tubes were quantified with ImageJ from a fixed size region-of-interest (ROI). The measured values were normalized

against a sample of HEPES-buffer and plotted against the sample concentration. Relaxation times (TR) between 100 to 3000 ms were screened for the Gd-doped MSNs. For quantitative ROI analysis, MR images with TR of 400 ms were used.

Results and discussion

Synthesis of MSNs and incorporation of gadolinium ions into MSN matrices

MCM-41 type regular pore-sized MSNs and pore-expanded hollow-structured MSN (H-MSN) were synthesized according to the protocols described in the M&M section, and subsequently subjected to either calcination or solvent extraction as SDA removal methods. According to our previous study, the aminosilane (APTES) is crucial for the formation of the hollow structure; whereby, in order to make the regular MSN matrix comparable with the H-MSN matrix, also regular MSNs were prepared by using similar amounts of APTES. Noteworthy, depending on the SDA removal method, the incorporated amino groups will be removed (calcination) or preserved (solvent extraction). Afterwards, two different routes were followed for the incorporation of paramagnetic centers into the MSN matrices, as shown in Scheme 2a and Scheme 2b above. The first route is based on doping of gadolinium ions from two different gadolinium sources, either by introducing gadolinium into the synthesis solution of MSNs (*in situ* synthesis) or, as a second approach, after the MSNs have been prepared (post synthesis). The aim of the different synthesis protocols and post synthesis treatments for SDA removal (solvent extraction and calcination) were to provide evenly distributed gadolinium paramagnetic centers within the MSN matrices, which could, in turn, provide optimal water accessibility of the Gd centers while preserving the morphology of pristine MSNs for further applications.

Characterization of MSNs before and after gadolinium incorporation

The changes in morphology of MSN and H-MSN before and after the *in situ* synthesis $GdCl_3$ and $Gd(acac)_3$ doping protocols were investigated with SEM in order to observe possible defects on the MSN morphology with the addition of gadolinium salts into the synthesis solutions. As shown in Figure 1, addition of $GdCl_3$ to the synthesis solution (*in situ* synthesis doping) of MSN and H-MSN disturbs the growth of the particles (Figure 1b and Figure 1e) whereas such a degree of disturbance was not observed when $Gd(acac)_3$ was employed as the gadolinium source (Figure 1c and Figure 1f).

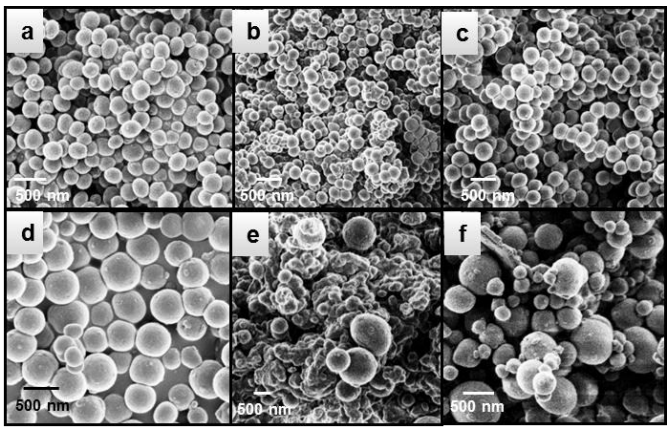

Figure1. SEM images of a) $[MSN]_{cal.}$ b) $[MSN]_{cal.}$: $(Gd(Cl)_3)_{in\ situ}$ c) $[MSN]_{cal.}$: $(Gd(acac)_3)_{in\ situ}$ d) $[H\text{-}MSN]_{cal}$ e) $[H\text{-}MSN]_{cal.}$: $(Gd(Cl)_3)_{in\ situ}$ f) [H-MSN]cal. : $(Gd(acac)_3)_{in\ situ}$

The observed morphology disturbance could be related to the difference between the complex stability of $Gd(acac)_3$ and $GdCl_3$. Even if both $GdCl_3$ and $Gd(acac)_3$ complexes have the same coordination number 3, they have different denticity. The chloride ligand has monodenticity, whereas the acetylacetone ligand ($CH_3C(O)CH_2C(O)CH_3$) binds from two sides to gadolinium through its both oxygen atoms. As is well-known, complexes of polydentate ligands tend to be more stable compared to complexes derived from monodentate ligands. Therefore, less stable $GdCl_3$ can dissociate better than $Gd(acac)_3$ and disturb the sol-gel process formation of MSNs. Especially when the high pH (pH~11) of the synthesis solution is considered, Gd (III) rare earth metal from $GdCl_3$ complex might form gadolinium hydroxide, that could affect the condensation reactions in the sol-gel kinetics, which can easily lead to disturbance in the MSN formation. Conversely, the applied post synthesis doping protocols did not cause any changes in the morphology of MSNs as the MSN was already formed upon addition of the gadolinium sources.

The further structural investigation of prepared MSNs, before starting the post synthesis doping of gadolinium into MSN and H-MSN matrices, was investigated by powder X-ray (PXRD) diffraction analysis to detect the possible defects in mesoscopic ordering of MSNs that might be caused during the post synthesis doping process. For this purpose, the pristine solvent extracted and calcined MSN ($[MSN]_{extr.}$, $[MSN]_{cal.}$) and H-MSN matrices ($[H\text{-}MSN]_{extr.}$, $[H\text{-}MSN]_{cal.}$) were treated under the same conditions as those applied for the post synthesis doping protocol (30 minutes sonication, 2.5 h mixing in HEPES buffer as dispersion) without the addition of any gadolinium sources. Distortion of the mesoscopic order of the MSNs might affect the water accessibility to gadolinium centers in the matrices negatively upon application. The patterns are presented in view of the effect of the SDA removing protocols (Figure 2) and the employed post synthesis doping protocols utilizing both gadolinium sources ($GdCl_3$, $Gd(acac)_3$) and their effect on the mesoscopic order of MSN and H-MSN. As shown in the diffractograms (Figure 2), the calcination process for SDA removal provides better rigidity for both MSN matrices. The partial distortion of the pore ordering was observed for

the matrices treated by the solvent extraction process, which is most probably due to accelerated dissolution rate of silica caused by the existing amine groups and, furthermore, the lower silica condensation degree, when exposed to aqueous media.[35,46]

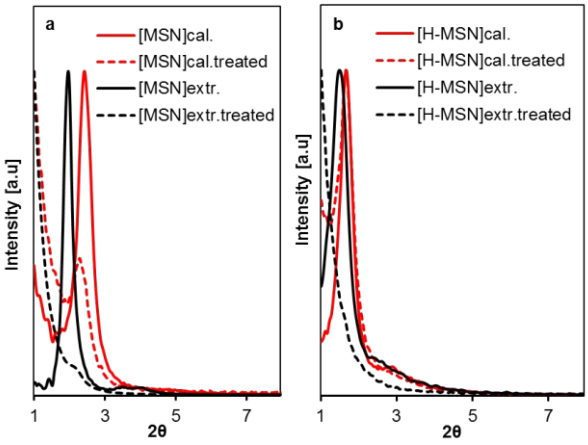

Figure 2. PXRD patterns of (a) calcined /solvent extracted MSN powders ($[MSN]_{cal.}$,$[MSN]_{extr.}$),and after treating them under the same conditions of the post synthesis doping protocol ($[MSN]_{cal.}$treated , $[MSN]_{extr.}$treated) (b) calcined /solvent extracted H-MSN powders ($[H\text{-}MSN]_{cal.}$,$[H\text{-}MSN]_{extr}$), and after treating them under the same conditions of the post synthesis doping protocol ($[H\text{-}MSN]_{cal.}$treated , $[H\text{-}MSN]_{extr.}$treated)

The changes in mesostructural ordering of MSNs were also observed as an influence of the different doping protocols presented in Supplementary Figure S1. A clear difference was observed between *in situ* synthesis and post synthesis doped MSNs. The *in situ* synthesis doping of $Gd(Cl)_3$ resulted in significant disturbance of the mesostructural order of $[MSN]_{cal.}$: $(GdCl_3)_{in\ situ}$, whereas such an influence was not observed for $[MSN]_{cal.}$: $(Gd(acac)_3)_{in\ situ}$, $[H\text{-}MSN]_{cal.}$: $(Gd(Cl)_3)_{in\ situ}$ and $[H\text{-}MSN]_{cal.}$: $(Gd(acac)_3)_{in\ situ}$. The observed differences could also be a result of the variations in the concentration of added gadolinium salt into the sol-gel synthesis process, as was discussed above; and was also evident from the SEM image results. Hence, the presented diffractograms (Figure S1**)** and corresponding electron microcopy images confirm that the post synthesis doping protocol does not lead to any distortion in the calcined MSN matrix structure or morphology, which is also an additional advantage in considering the multifunctional MSN concept, since the well-defined structural properties of MSNs can be preserved the same as pristine MSNs.

After investigation of the structural and morphological alterations in the prepared MSN series, the changes in the dispersibility and net surface charge was determined by measuring the hydrodynamic diameter and zeta potential values of the samples in suspension form. The samples were thus dispersed in HEPES buffer (to a concentration of 0.5 mg/mL) for the measurements, and poly(ethylene glycol)-poly(ethylene imine) (PEG-PEI) block copolymer, which was also employed in our *in vitro* evaluations in order to enhance the cellular uptake,[1] was further used here as dispersing agent in order to obtain better dispersibility of the MSN-based contrast agents under physiological/biological conditions.[47,48] The obtained values for the measurements are presented in Table 1. As shown in the table, the hydrodynamic diameters and the zeta potential values of the produced samples are varying between 300-700 nm and highly negative (approx. -41 mV) and positive values (approx. +17 mV) due to the different gadolinium incorporation routes as well as an abundance of amine groups on the MSNs, provided by the added amino silane reagent in the synthesis process.

As a brief summary of the characterization part, the post synthesis doping of $[MSN]_{cal.}$ and $[H\text{-}MSN]_{cal.}$ matrices preserves the structure of pristine MSNs and cause the least defects compared to the other preparation routes, while the morphology, polydispersity index (PDI) and hydrodynamic size of MSNs remain almost the same as pristine MSNs, which are important factors for their further application.

Table 1. Hydrodynamic diameter and zeta potential values of prepared MSNs in HEPES buffer (pH 7.2, 25mM) as 0.5 mg/mL particle suspensions (Zeta potential measurements were carried out before adding the dispersion agent, a PEG-PEI copolymer)

SAMPLE	Hydrodynamic size [nm]	PDI	Zeta Potential [mV]
$[MSN]_{cal.}$	313	0.27	-39
$[MSN]_{extr.}$	530	0.32	17
$[H\text{-}MSN]_{cal.}$	686	0.26	-32
$[H\text{-}MSN]_{extr.}$	650	0.43	4
$[MSN]_{cal.}$: $(Gd(Cl)_3)_{in\ situ}$	417	0.65	-31
$[MSN]_{cal.}$: $(Gd(aca)_3)_{in\ situ}$	329	0.3	-41
$[H\text{-}MSN]_{cal.}$: $(Gd(Cl)_3)_{in\ situ}$	775	0.53	-28
$[H\text{-}MSN]_{cal.}$: $(Gd(aca)_3)_{in\ situ}$	574	0.42	-32
$[MSN]_{cal.}$: $(Gd(Cl)_3)_{post}$	243	0.1	-14
$[MSN]_{extr.}$: $(Gd(Cl)_3)_{post}$	381	0.38	16
$[MSN]_{cal.}$: $(Gd(aca)_3)_{post}$	348	0.34	-32
$[MSN]_{extr.}$: $(Gd(aca)_3)_{post}$	283	0.12	16
$[H\text{-}MSN]_{cal.}$: $(Gd(Cl)_3)_{post}$	671	0.29	-23
$[H\text{-}MSN]_{extr.}$: $(Gd(Cl)_3)_{post}$	348	0.3	4
$[H\text{-}MSN]_{cal.}$: $(Gd(aca)_3)_{post}$	650	0.35	-25
$[H\text{-}MSN]_{extr.}$: $(Gd(aca)_3)_{post}$	730	0.34	-2

Determination of incorporated gadolinium amount in MSNs

The quantitative determination of the amount of doped gadolinium in MSN matrices was carried out by ICP-AES after complete dissolution of the samples in HF. The results have been plotted in Figure 3 and given in Table 2 below, from which can be concluded that the highest incorporation of gadolinium was obtained via post synthesis doping of $[MSN]_{extr.}$ and $[H\text{-}MSN]_{extr.}$ matrices with $Gd(Cl)_3$ (0.81 µmol Gd / mg of $[MSN]_{extr.}$: $(Gd(Cl)_3)_{post}$ and 0.92 µmol/mg of $[H\text{-}MSN]_{extr.}$: $(Gd(Cl)_3)_{post}$). The second highest gadolinium accumulation was obtained via post synthesis doping of $[MSN]_{cal.}$ and $[H\text{-}MSN]_{cal.}$ matrices with $Gd(Cl)_3$ (0.70 µmol Gd / mg of $[MSN]_{cal.}$: $(Gd(Cl)_3)_{post}$ and 0.60 µmol/mg of $[H\text{-}MSN]_{cal.}$: $(Gd(Cl)_3)_{post}$

Besides this, no significant distinctions were obtained for the post synthesis doping of $Gd(acac)_3$ for either of these matrices *via* both SDA removal protocols (0.53 µmol Gd/mg of $[MSN]_{extr.}$: $(Gd(acac)_3)_{post}$ and 0.50 µmol/mg of $[H\text{-}MSN]_{extr.}$: $(Gd(acac)_3)_{post}$ 0.52 µmol Gd/mg of $[MSN]_{cal.}$: $(Gd(acac)_3)_{post}$ and 0.52 µmol/mg of $[H\text{-}MSN]_{cal.}$: $(Gd(acac)_3)_{post}$). The least amount of gadolinium incorporation was obtained with the $Gd(aca)_3$ *in situ* synthesis doping protocol ($[MSN]_{cal.}$/$[H\text{-}MSN]_{cal.}$: $(Gd(acac)_3)_{in\ situ}$) as expected. Considerably higher accumulation of gadolinium for $[MSN]_{cal.}$: $(Gd(Cl)_3)_{in\ situ}$ and $[H\text{-}MSN]_{cal.}$: $(Gd(Cl)_3)_{in\ situ}$ preparation compared to $[MSN]_{cal.}$: $(Gd(acac)_3)_{in\ situ}$ $[H\text{-}MSN]_{cal.}$: $(Gd(acac)_3)_{in\ situ}$ also point to the implications of the observed alteration in the morphology differences due to denticity difference of $GdCl_3$ and $Gd(acac)_3$ as presented in the characterization part.

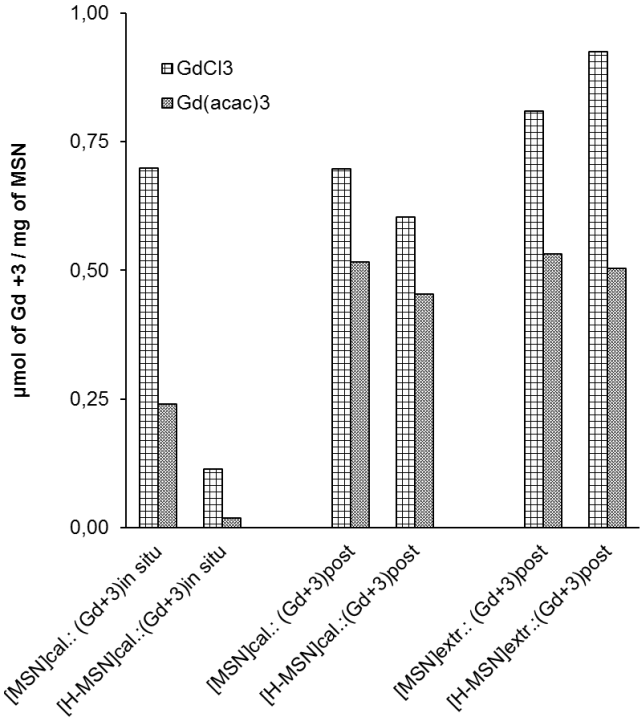

Figure 3. The determined gadolinium amount in MSN based contrast agents prepared via *post synthesis* and *in situ synthesis* doping routes.

Relaxivity properties of prepared MSNs

The relaxivity values of the differently prepared MSN-based contrast agents were determined by suspending the samples in distilled water at different concentrations (in the range of 0.01-10 mg/mL) and thereafter measuring the longitudinal proton relaxation times (T_1) and transverse relaxation times (T_2) of the suspensions at 37°C. First, the performance of all the samples was investigated by plotting T_1^{-1} values vs. MSN concentration. The presented plots (Figure 4) show that post synthesis doping of gadolinium of calcined matrices leads to better reciprocal T_1 (T_1^{-1}) increase and longitudinal relaxivity (r_1) enhancement with increasing sample concentration compared to *in situ* synthesis gadolinium doped MSNs. This might be caused by the colloidal stability restrictions with increasing MSN concentration for the other samples, leading to deviation from linearity in the relaxivity plots. The samples prepared *via* doping of $GdCl_3$ ($[MSN]_{cal.}$:$(Gd(Cl)_3)_{in\ situ}$, $[MSN]_{cal.}$:$(Gd(Cl)_3)_{post}$, $[MSN]_{extr.}$:$(Gd(Cl)_3)_{post}$) resulted in sedimentation when the concentration of the samples were increased above 2 mg/mL, which is possibly due to lack of proper stabilization mechanisms being operative in the suspension at higher concentrations. On the other hand, among the samples prepared by $Gd(acac)_3$ doping, such sedimentation was observed only for $[MSN]_{extr.}$:$(Gd(acac)_3)_{post}$ above 2 mg/mL concentration, while for the rest of the samples good dispersion stability was observed also above 2 mg/mL.

By considering the measurements up to 2 mg/mL particle concentrations i.e. before deviation from linearity started to occur, from Figure 4, the superior route of preparation for obtaining the best T_1 contrast agent was deduced from the relaxivity data listed in Table 2, for which the plots are given in the supporting information Figure S2 and Figure S3. Quite remarkably, the H-MSN samples show pronouncedly better longitudinal, r_1 values compared to their corresponding regular MSN matrices. Especially when the longitudinal relaxivity values, r_1, of the *in situ* synthesis preparations were compared, considerable differences were obtained between H-MSN and regular MSN matrices. $Gd(Cl)_3$ *in situ* synthesis doped H-MSN ($[H\text{-}MSN]_{cal}$: $(GdCl3)_{in\ situ}$, 6.75 $mM^{-1}\ s^{-1}$) resulted in 20-fold increase in r_1 values compared to $Gd(Cl)_3$ *in situ* synthesis doped regular MSN ($[MSN]_{cal}$: $(GdCl_3)_{in\ situ}$, 0.31 $mM^{-1}s^{-1}$) despite that the lowest Gd (0.1 µmol in mg of H-MSN) incorporation was obtained for ($[H\text{-}MSN]_{cal}$: $(GdCl_3)_{in\ situ}$ among all the employed protocols. This should mainly be due to the structural differences of the matrices. Namely, the pore-expanded hollow mesoporous silica nanoparticle structure (H-MSN) definitely seems to aid in achieving better diffusion of water molecules throughout these matrices to interact with the accommodated paramagnetic gadolinium centers. For the $Gd(acac)_3$ *in situ* synthesis doped MSN preparations, the same effect was also observed with 17-fold increase in the longitudinal relaxivity value (r_1) between the hollow and the regular counterparts.

The matrix structure-dependent variations were not observed for the samples prepared by post synthesis doping protocols. Here, the differences were mainly observed between solvent extracted and calcined matrices within the same structure series of MSNs. Even if more gadolinium was accommodated into the solvent-extracted MSN matrices compared to the calcined MSNs, post synthesis gadolinium doping of solvent extracted MSN matrices (both $[MSN]_{extr.}$ and $[H\text{-}MSN]_{extr.}$) resulted in lower r_1 values compared to post synthesis gadolinium doping on calcined MSN matrices (both $[MSN]_{cal.}$ and $[H\text{-}MSN]_{cal.}$). The plausible explanation for such an observation could be the variability in the mesoscopic ordering of MSNs, which was already pinpointed in the diffraction patterns in Figure 2 as destruction of mesoporous ordering upon the post synthesis doping of gadolinium into solvent extracted MSN matrices. Accommodated organic groups on

the solvent extracted MSN surfaces ([MSN]$_{extr.}$ and [H-MSN]$_{extr.}$), which were incorporated via co-condensation of the employed aminosilane (aminopropyltriethoxysilane silane, APTES), may have an influence on obtaining lower r_1 values.

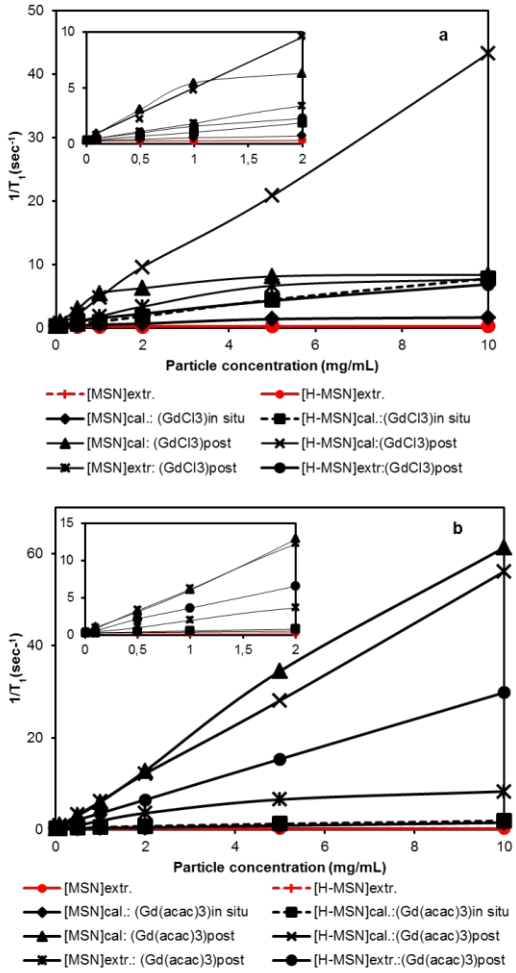

Figure 4. The longitudinal relaxation time T_1 vs. concentration of MSN based contrast agent suspensions prepared with increasing particle concentrations up to 10 mg/mL, and insets up to 2 mg/mL a) $GdCl_3$ doped MSNs and b) $Gd(acac)_3$ doped MSNs.

Namely, the incorporation of organic amino groups is believed to lead to a higher amount of gadolinium accommodation, which causes significant dipole-dipole interactions with the metal ions, which, in turn, shortens the relaxation times.[49] As a result of longitudinal relaxivity (r_1) and transversal relaxivity (r_2) values, as well as calculations according to Table 2 below, the most promising MSN based T_1 contrast agents can be affirmed as [H-MSN]$_{cal}$: (Gd(acac)$_3$)$_{post}$) with both a low r_2/r_1 ratio of 1.6 as well as the highest r_1 relaxivity value 13.1 mM^{-1} s^{-1}. Here, the r_2/r_1 ratio is an indication of the type (T_1, T_2) of contrast agent and the criterion is defined by the ratio between the r_2 and r_1 values (r_2/r_1). For contrast agents, an r_2/r_1 value from 1.1 to 2.0 is attributed as a T_1 type contrast agent, and over 2.0 is typically T_2 type contrast agents.[50] The reason for the varying r_2/r_1 ratios in Table 2 may be related to the amount as well as distribution of Gd within the matrices, whereby Tseng *et al*. has pointed out that when the concentration of Gd becomes too high, the T_2 relaxation effect will overcome the T_1 effect, thus suppressing the T_1 signal.[51]

Table2. Longitudinal relaxivity (r_1) and transverse relaxivity (r_2) data of prepared MSN-based contrast agents

SAMPLES	Gd^{+3} amount in MSNs/ μmol mg^{-1}	r_1 / mM^{-1}s^{-1}	r_2 / mM^{-1}s^{-1}	r_2/r_1
[MSN]$_{cal}$: (Gd(Cl)$_3$)$_{in\ situ}$	0.7	0.3	1.5	5
[H-MSN]$_{cal.}$:(Gd(Cl)$_3$))$_{in\ situ}$	0.11	6.7	10.2	1.5
[MSN]$_{cal}$: (Gd(acac)$_3$)$_{in\ situ}$	0.69	0.5	2.6	5.2
[H-MSN]$_{cal.}$:(Gd(acac)$_3$))$_{in\ situ}$	0.6	13.1	28.4	2.2
[MSN]$_{cal.}$: (Gd(Cl)3)$_{post}$	0.81	7.3	12.1	1.6
[MSN]$_{extr.}$ (Gd(Cl)3)$_{post}$	0.92	1.9	5.6	2.9
[H-MSN]$_{calc}$:(Gd(Cl)$_3$)$_{post}$	0.24	7.7	12.8	1.7
[H-MSN]$_{extr.}$:(Gd(Cl)$_3$)$_{post}$	0.02	1.0	3.3	3.3
[MSN]$_{cal.}$: (Gd(acac)$_3$)$_{post}$	0.52	12.1	17.7	1.5
[MSN]$_{extr.}$ (Gd(acac)$_3$)$_{post}$	0.45	2.4	7.5	3.1
[H-MSN]$_{calc}$:(Gd(acac)$_3$)$_{post}$	0.53	13.1	21.1	1.6
[H-MSN]$_{extr.}$:(Gd(acac)$_3$)$_{post}$	0.5	5.9	13.1	2.2

XPS and XRD analysis of MSN-based contrast agents

As a further investigation for explaining the significant enhancement in the relaxivity values for certain samples, especially for the pore-expanded hollow MSN (H-MSN) structure, the localization of the paramagnetic centers in the matrix was evaluated. For this reason, we carried out X-ray photoelectron spectroscopy (XPS) analysis. Thus, the chemical composition of incorporated gadolinium content *via* the post synthesis and *in situ* synthesis doping routes for the H-MSN matrices were investigated. In Table 3, the binding energies for the concerned element's photoelectron peaks of the *in situ* and post synthesis doped H-MSN matrices and starting $GdCl_3{\cdot}6H_2O$ and $Gd(acac)_3{\cdot}2H_2O$ reagents are presented by considering the C1s peak with binding energy of 284.8 eV as reference, showing that the instrument is calibrated. According to this table and the given photoelectron peak of analyzed samples in supporting figures Figure S4, no Gd peak was observed for the *in situ* synthesis Gd doped H-MSN preparation, even if it exhibited the highest r_1 values in the relaxivity measurements. Since XPS is a surface sensitive technique, and the measurement depth is limited to 10 nm, the reason for such an observation should be a result of either low gadolinium content at the surface of the *in situ* synthesis doped H-MSN, or a deeper than 10 nm incorporation of gadolinium into the H-MSN framework. In addition, when the O1s peak (given in supporting Figure S5) of starting Gd sources and *in situ* synthesis doped H-MSN material were compared, no significant shift in the peak position or the shoulder formation was observed, in accordance to previous studies of gadolinium incorporated mesoporous silica nanoparticles.[52] The observations from XPS and relaxivity measurements for *in situ* synthesis doped H-MSN ([H-MSN]$_{cal}$: (GdCl$_3$)$_{in\ situ}$ and [H-MSN]$_{cal}$: (Gd(acac)$_3$)$_{in\ situ}$) indicate that the accommodation of Gd(III) is mainly in the interior section of the H-MSN particle, which allows for better possibility for water molecules to access the paramagnetic centers with the provided water confinement effect.[17,52] Further, the low degree of gadolinium

accommodation prevents the shortening of the electronic relaxations due to the absence of dipole-dipole interactions, which resulted in better r_1 values as compared to regular pore-sized MSN preparations ($[MSN]_{cal}$: $(GdCl_3)_{in\ situ}$ and $[MSN]_{cal}$: $(Gd(acac)_3)_{in\ situ}$).

Table3. Binding energies of Si, O, Gd elements on the *in situ* and post synthesis doped H-MSN matrices.

SAMPLE	Si 2p	O 1s	Gd $4d_{3/2}$	Gd $4d_{5/2}$
$GdCl_3.6H_2O$	-	532.4	148.8	143.7
$Gd(aca)_3.2H_2O$	-	531.4	148.6	142.7
$[H\text{-}MSN]_{cal}$.:$(Gd(Cl)_3)_{in\ situ}$	104.0	533.4	-	-
$[H\text{-}MSN]_{cal}$.:$(Gd(acac)_3)_{in\ situ}$	104.0	533.4	-	-
$[H\text{-}MSN]_{cal}$.:$(Gd(Cl)_3)_{post}$	103.1	532.3	148.5	142.5
$[H\text{-}MSN]_{cal}$.:$(Gd(acac)_3)_{post}$	103.2	532.5	148.5	142.5
$[H\text{-}MSN]_{extr.}$.:$(Gd(Cl)_3)_{post}$	102.9	532.3	148.5	142.6
$[H\text{-}MSN]_{extr.}$.:$(Gd(acac)_3)_{post}$	103.0	532.3	148.5	142.2

For the post synthesis doped samples, double peaks were obtained for Gd 4d, which are mainly attributed as Gd $4d_{3/2}$ and Gd $4d_{5/2}$ peaks.[53, 46] The observed shift to slightly lower binding energy values for Gd $4d_{5/2}$ (from 143.7 to 142.5 eV) with the post synthesis doping utilizing $GdCl_3.6H_2O$ as Gd-source, is probably related to the interaction of Gd atoms with Si within the doped H-MSN matrix. The binding energy value for Gd $4d_{5/2}$ remained the same upon doping with $Gd(acac)_3$, which signifies the interaction Gd atoms is slightly weaker than for the $GdCl_3$ post synthesis doped H-MSN matrix. In order to further evaluate the differences on the surfaces of the H-MSN matrices attributed to Gd doping, we investigated the alterations in Si 2p peaks. The observed peak shifts for Si 2p (Supplementary Figure S6) assign the variations in the interaction strengths between Gd, O and Si atoms. As shown in the table, post synthesis doping into the $[H\text{-}MSN]_{extr.}$ matrix resulted in a shift in the Si 2p and O 1s peak positions to around 1 eV lower binding energy values compared with the *in situ* synthesis doping route, which also indirectly indicate that the existing gadolinium is mainly accommodated at the exterior surface of MSN matrices prepared via the post synthesis doping routes.

All in all, from the XPS analysis, we can deduce that the strongest interactions between gadolinium and H-MSN was obtained for the $[H\text{-}MSN]_{extr.}$: $(GdCl_3)_{post}$ sample, whereas gadolinium is mainly accommodated in the interior part of H-MSN when introduced via the *in situ* synthesis doping route. The strong interaction between doped Gd and a mesoporous silica matrix has indeed been verified by Shao *et al.*[23] who found the bonding behavior was a combination of ionic and covalent nature, based on density functional theory (DFT) calculations.

Furthermore, in order to prove the absence of any re-crystallization of the gadolinium salts on the hollow-structured and pore expanded hollow MSN matrices (H-MSN), which could negatively affect the even distribution of gadolinium within the MSN matrices, X-ray diffraction analysis was carried out. The absence of peaks in the high–angle portion of the XRD pattern presented in Figure 5 proves that no crystalline structure formation with neither *in situ* nor post synthesis doping protocols occurred.

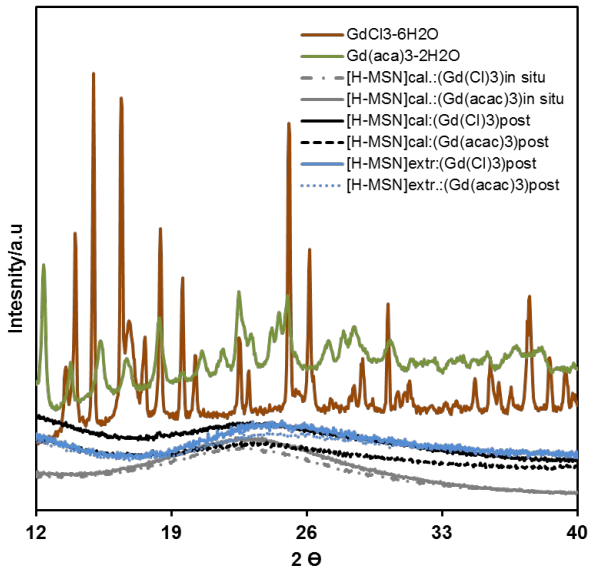

Figure 5. X-ray diffaraction pattrens of H-MSN based contrast agent powder after incorporation of gadolinium

***In vitro* cytocompatibility of MSNs**

In the materials characterization part, the $[H\text{-}MSN]cal:(Gd(acac)_3)_{post}$ preparation resulted in the shortest longitudinal proton relaxation time (*T*1) and the best r_1 relaxivity value. This route of preparation also preserved the mesoscoping order of the $[H\text{-}MSN]_{cal}$ matrix, whereby the hydrodynamic size and dispersibility of the sample ($[H\text{-}MSN]cal: (Gd(acac)_3)_{post}$) remained on a level comparable to pristine $[H\text{-}MSN]_{cal.}$ To examine the performance of the ([H-MSN]cal: (Gd(acac)3)post) contrast agent (CA) in a biological environment, we first wanted to test the cytocompatibility of this potential MSN-based CA. WST-1 assay was performed at different particle concentrations (10, 25, 50 µg/ml) for 48h (Figure 6) to determine cell viability upon particle incubation with cells. The selected MSN-based CAs were coated with in-house produced mPEG-PEI copolymer in order to facilitate cellular uptake, according to our previous findings.[45] No obvious negative effect on cell viability was found at the studied concentrations (Figure S7).

It is noteworthy that the toxicity level of Gd^{3+} has been reported as 1 mM for HeLa cells,[54] and in our case, assuming a cellular uptake of 100 %, the highest used Gd^{3+} concentration in the cells would be 30 µM. Hence, utilizing the MSN based contrast agents with the optimized structural design can reduce the amount of gadolinium exposure.

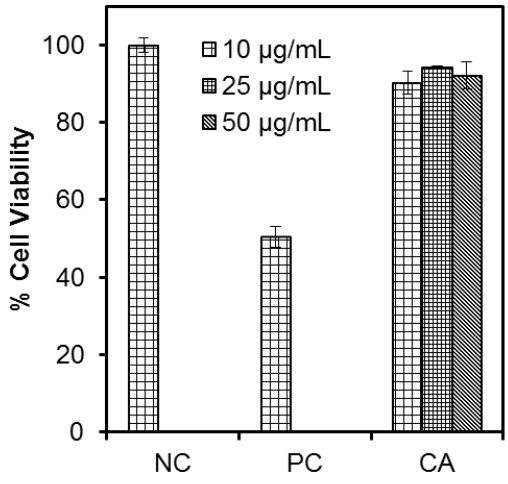

Figure6. *In vitro* dose dependent cell viability data of [H-MSN]$_{cal.}$:(Gd(acac)$_3$)$_{post}$ contrast agent after 48 h incubation time on HeLa cell line

Phantom and tumor imaging on CAM

As the final proof of concept to demonstrate the potential of the Gd^{3+}-doped MSN as CAs, magnetic resonance imaging (MRI) was performed on a standard clinical MRI-scanner. HeLa cells were labeled with the selected CA [[H-MSN]$_{cal}$:(Gd(acac)$_3$)$_{post}$] sample at 0.1, 1.0, 10, 50 µg/ml concentrations. This sample was chosen due to its largest r_1 value 13.1 $mM^{-1}s^{-1}$, uniform dispersion and well-preserved structure among all the studied CAs. Thereafter, the labeled cells were immobilized into agar and the immobilized cells were subsequently scanned on a clinical 3 T MRI instrument. A clear signal enhancement compared to control was seen in three samples out of four. The 1 µg/ml sample did not show enhanced signal compared to the control, but instead showed an MR signal intensity compared to the blank specimen consisting of agar. This was later confirmed to be due to the cells being landed at the bottom of the tube and not distributed evenly across the agar solution compared to other specimens. Therefore, the ROI measurements (figure 7b) and visual inspection showed this sample to have an MR signal similar to agar (blank specimen) but not to the control. However, this was not an issue with the three other samples imaged with the clinical scanner as both visual (Figure 7a) and ROI vs concentration inspection at the relaxation time (TR) 400 ms for the labeled cells (Figure 7b).

The [H-MSN]$_{cal.}$:(Gd(acac)$_3$)$_{post}$ particles (50 µg/mL) were further used to label HeLa cells that were subsequently implanted onto the CAM of a chick embryo *in ova* as a model for *in vivo* imaging. The details are given in the supplementary information. After implantation, the tumor cells were allowed to grow for six days, after which the live embryos were terminated according to regulatory guidelines. *T1*-weighted 3D MR imaging was performed on the eggs with formed tumors labeled with CA prior to implantation. The control (implanted with non-labeled HeLa cells) and sample were imaged with similar MRI settings in the same imaging session. As presented in Figure 8, the labeled tumors were clearly visible as bright spots on top of the CAM. Most of the Gd-based contrast agents available for clinical usage typically applied as extracellular agents[55] (e.g. blood pool imaging), for which the plasma elimination half-life is short. Due to this reason, more efforts have recently been focused on developing Gd- based CAs for labelling of cells for tracking of cell-based therapies[56], where the cellular labeling is realized by phagocytosis or receptor-mediated endocytosis.[57] In this respect, clear detectability of our particulate CAs even a week after exposure to a biological system (one day cell labeling + six days tumor formation of labeled cells) is interesting, especially when regarding the shortcomings of clinically used (molecular) Gd-based CAs, i.e. short half-lives in the body due to extracellular existence and their molecular form. To address these existing shortcomings, additional *in vivo* tests are also planned as a continuation of this study, together with the evaluation of Gd biodistrubition in murine *in vivo* models both after IV administration as well as when used as cellular labels.

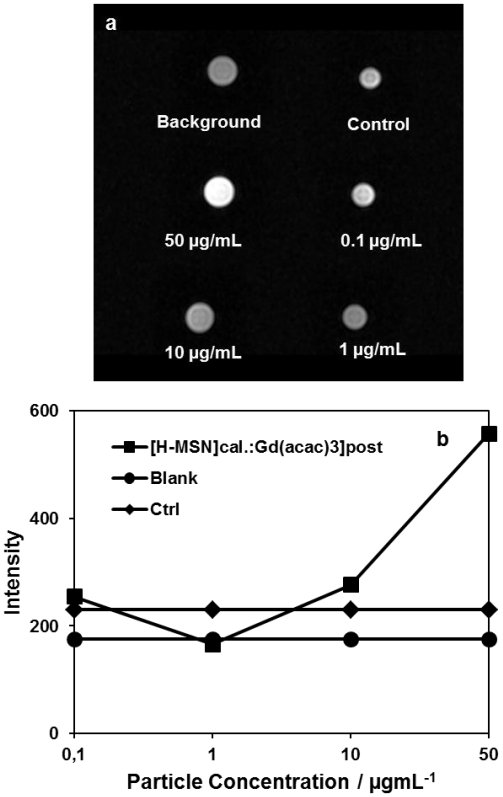

Figure 7. a) T1-weighted phantom images of cells labeled with [H-MSN]$_{cal.}$:(Gd(acac)$_3$)post contrast agent (r_1:13.1 $mM^{-1}s^{-1}$) b) corresponding signal intensities for ROI vs concentration at the relaxation time (TR) 400 ms.

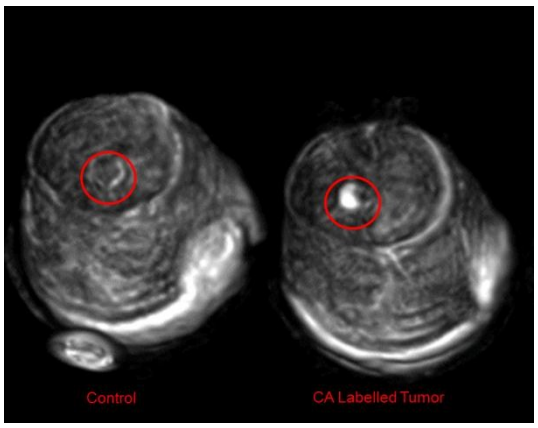

Figure 8. The best CA candidate ([H-MSN]$_{cal}$: (Gd(acac)$_3$)$_{post}$) was used to label HeLa cancer cells, which were then implanted over CAM. The labelled tumors were clearly visualized *in ova* six days after implantation in the acquired MR images of the whole egg.

Conclusions

In summary, the contrast enhancement of Gd (III) incorporated nanoparticle-based contrast agents by the modulation of preparation and structural parameters of mesoporous silica nanoparticles (MSNs) were comprehensively explored. According to our investigation, when the structural variations of the MSN matrix were considered, the *in situ* incorporation route helps to increase the longitudinal relaxivity value (r_1) of hollow pore-expanded MSNs (H-MSN). Employing these approaches for Gd incorporation and structural considerations, resulted in roughly 20-fold higher value compared to the corresponding regular pore-sized MSN; alas while simultaneously causing the highest degree of destruction on the particle morphology. On the other hand, structure dependent variation was not pronounced for the post synthesis preparation route. Instead, for the post synthesis preparation route, the most effective r_1 value enhancement was provided with the modulation of the SDA removal method. The calcination process resulted in almost 6-fold higher r_1 values as compared to solvent-extraction of the corresponding MSN matrix. Therefore, while the structural variation of the MSN matrix creates significant r_1 enhancement in the *in situ* synthesis preparations, it remains the secondary regulator for the post synthesis preparation route. As a consequence, the best CA candidate was prepared by post synthesis doping of a calcined hollow MSN matrix with Gd(acac)$_3$ ([H-MSN]$_{cal}$:(Gd(acac)$_3$)$_{post}$). This procedure yielded a CA candidate with a relaxivity value of 13.1 $mM^{-1}s^{-1}$, which is approximately four-fold to clinically used Gd-based molecular CAs, and a r_2/r_1 ratio of 1.6, rendering it predominantly a T_1 contrast agent. Ultimately, cells tolerated this most promising MSN-based CA candidate well, reducing the needed concentration of Gd (III) to 30 µM; whereby both labeled cells and tumors could be successfully imaged on a clinical 3T MRI scanner, the latter one week after exposure to and implantation into a biological system.

Acknowledgements

The authors would like to acknowledge Linus Silvander for SEM imaging, Sten Lindholm for ICP-AES analysis, Neeraj Prabhakar for assisting with *in ovo* experiments, LSK Poultry Oy, 23800 Laitila, Finland for providing chicken eggs. Financial contribution from Academy of Finland project #260599 is greatly acknowledged.

References

1 Z.R. Stephen, F.M. Kievit, and M. Zhang, *Materials Today* 2011, **14**, 330-338.
2 H.B. Na, I.C. Song, T. Hyeon, *Advanced Materials*, 2009, **21**, 2133-2148.
3 S. Flacke, S.Fischer, M.J. Scott, R.J. Fuhrhop, J.S. Allen, M. McLean, P. Winter, G.A. Sicard, P.J. Gaffney, S.A. Wickline, G.M. Lanza, *Circulation*, 2001, **11**, 1280-1285
4 H.Jaccard, P. Miéville, C. Cannizzo, C.R. Mayer, L. Helm, *Journal of Biological Inorganic Chemistry*, 2014, **19**, 145-159
5 J.C. Frias, Y. Ma, K.J. Williams, Z.A. Fayad, E.A. Fisher, *Nano Letters*, 2006, **6**, 2220-2224
6 K.M. Taylor, J.S. Kim, W.J. Rieter, H. An, W. Lin, W. Lin, Journal of American Chemical Society, 2008, 130, 2154-2155.
7 H. Yang, S. Santra, G.A. Walter, P.H. Holloway, *Advanced Materials*, 2006, **18**, 2890.
8 F. Carniato, L. Tei, W. Dastru, L. Marchese, M. Botta, *Chemical Communications*, 2009, 1246.
9 J.L. Vivero-Escoto, K.M.L. *T*aylor –Pashow, R.C.Huxford, J.D.Rocca, C.Ohoruwa, H.An, W.Lin, W.Lin, *Small*, 2011, 3519-3528
10 M. A. Bruckman, X. Yu, N. F. Steinmetz, *Nanotechnology,* 2013, **24**, 462001.
11 K.M.L Taylor-Pashow, J. D. Rocca, W. Lin, *Nanomaterials*, 2012, **2**, 1-14
12 Y-Z. Shao, L.-Z. Liu, S.-Q. Song, R.H. Cao, H. Liu, C.-Y. Cui, X.Li, M.-J. Bie, L. Li, *Contrast Media& Molecular Imaging*, 2011, **6**, 110-118.
13 Y. Shen, Y. Shao, H. He, Y. Tan, X. Tian, F. Xie, L. Li, *International Journal of Nanomedicine*, 2013, **8**, 119.
14 Y. Chen, H. Chen, S. Zhang, F. Chen, L. Zhang, J. Zhang, M. Zhu, H. Wu, L. Guo, J. Feng, J. Shi, *Advanced Functional Materials*, 2011, **21**, 270-278
15 J.Zhang, J.M.Rosenholm, *Therapeutic Delivery*, 2015, **6**, 891–893.
16 S. Shi, F. Chen, W. Cai, Nanomedicine, 2013, **8**, 2027-2039.
17 Zhang, J. M. Rosenholm, H. Gu, *ChemPhysChem*, 2012, **13**, 2016-2019.
18 K.R. Hurley, Y.-S. Lin, J. Zhang, S.M. Egger, C.L. Haynes, *Chemistry of Materials*, 2013, **25**, 1968 -1978.
19 Y. Chen, H. Chen, S. Zhang, F. Chen, S. Sun, Q. He, M. Ma, X. Wang, H. Wu, L. Zhang, *Biomaterials*, 2012, **33**, 2388-2398
20 Y. Chen, Q. Yin, X. Ji, S. Zhang, H. Chen, Y. Zheng, Y. Sun, H.Qu, Z. Wang, Y. Li, X. Wang, K. Zhang, L. Zhang, J. Shi, *Biomaterials*, 2012, **33**, 7126-7137
21 F. Stallmach, J. Kärger, C. Krause, M. Jeschke, U. Oberhangemann, *Journal of the American Chemical Society*, 2000, **122**, 9237-9242.
22 S. Yingying, S. Yuanzhi, H. Hoaqiang, T. Yunpu, T. Xiumei, X. Fukang, L. Li, *International Journal of Nanomedicine*, 2013, **8**, 119.
23 Y. Shao, X. Tian, W. Hua, Y. Zhang, H.Liu, H.He, Y.Shen, F.Xie, *Biomatreials*, 2012, **33**, 6438-6446

24 R.Guillet-Nicolas, J.-L. Bridot, Y. Seo, M.-A. Fortin, F. Kleitz, *Advanced Functional Materials*, 2011, **21**, 4653-4662.
25 F. Carniato, L. Tei, A. Arrais, L. Marchese, M. Botta, *Chemistry- A European Journal*, 2013, **19**, 1421-1428.
26 J. J. Davis, W. Y. Huang, G. L. Davies, *Journal of Materials Chemistry*, 2012, **22**, 22848.
27 *A.D. Sherry, P-Caravan, R.E. Lenkinski, Journal of Magnetic Resonance Imaging, 2009, 30,1240-1248.*
28 Moreau, E. Guillon, J.-C. Pierrard, J. Rimbault, M. Port, M. Aplincourt, *Chemistry A European Journal*, 2004, **10**, 5218-5232.
29 A. Bianchi, L. Calabi, C. Giorgi, P.Losi, P.Mariani, P.Paoli, R.Patrizia, V.Barbara, V.Mario, *Dalton Transactions*,2000, **5**, 697-705
30 E. Brucher, A.D. Sherry, *Inorganic Chemistry*, 1990, 8, **29**, 1555-1559.
31 X. Wang, T. Jin, V. Comblin, A. Lopez-Mut, E. Merciny, J.F. Desreux*, Inorganic Chemistry,* 1992, **31**,1095-1099.
32 J. K. Hsiao, C. P. Tsai, T. H. Chung, Y. Hung, M. Yao, H. M. Liu, C. Y. Mou, C- S. Yang, Y. C. Chen, D. M. Huang, *Small*,2008, **4**, 1445-1452.
33 C. P. Tsai, Y. Hung, Y. H. Chou, D. M. Huang, J. K. Hsiao, C. Chang, Y. C. Chen, C. Y. Mou, *Small*, 2008, **4**, 186-191.
34 M. Laprise-Pelletier, M. Bouchoucha, J. Lagueux, P. Chevallier, R. Lecomte, Y. Gossuin, F. Kleitz, M.-A. Fortin, *J. Mater. Chem. B*, 2015, **3**, 748-758.
35 R. Boiteau, T. Meade, J. Major, *Nanoscape*, 2008, **5**, 32-39.
36 D. Desai, D. Sen Karaman, N. Prabhakar, S. Tadayon, A. Duchanoy, D. M. Toivola, S. Rajput, T. Näreoja, J. M. Rosenholm, *Mesoporous Biomaterials*, 2014, **1**, 16.
37 Y.Chen, H. Chen, J. Shi, *Advanced Materials*, 2013, **25**, 3144-3176.
38 Argyo, V. Weiss, C. Bräuche, T. Bein, *Chemistry of Materials*,2014, **26**, 435-451.
39 T. Wang, L. Zhang, Z. Su, C. Wang, Y. Liao, Q. Fu, *ACS Applied Materials & Interfaces*, 2011, **3**, 2479-2486.
40 Y.-K. Hwang, J.-N. Choi, J-H. Cho, H. Kwon, S. Huh, *European Journal of Inorganic Chemistry*, 2012, **2012**, 3379-3383.
41 J. Shin, R. Md Anisur, M.K. Ko, G. H. Im, J. H. Lee, I. S. Lee, *Angewandte Chemie*, 2009, 48, 321-324.
42 M. Bouchoucha, R. C. Gaudreault, M. A. Fortin, F. Kleitz, *Adv. Funct. Mater.,* 2014, 24, 5911- 5923
43 U. I. Tromsdorf, O.T. Bruns, S.C. Salmen, U. Beisiegel, H. Weller, *Nano Letters*, 2009 **9**, 4434-440.
44 D. Şen Karaman, D. Desai, R. Senthilkumar, E. Johansson, N. Råtts, M. Oden, J.E. Eriksson, C. Sahlgren, D.M. Toivola, J.M. Rosenholm, *Nanoscale Research Letters*, 2012, **7**, 358
45 D. Şen Karaman, T. Gulin-Sarfraz, J. Zhang, J.M. Rosenholm, *Materials Letters*, 2015, **143,** 140-143.
46 S. V. Patwardhan, G. E. Tilburey, C. C. Perry, *Langmuir*, 2011, **27**, 15135-15145
47 D. Şen Karaman, T. Gulin-Sarfraz, G. Hedström, A. Duchanoy, P. Eklund, J. M. Rosenholm, *Journal of Colloid and Interface Science*, 2014, **418**, 300-310.
48 N. Prabhakar, T. Näreoj, E. von Haartman, D. Şen Karaman, H. Jiang, S. Koho, T. A. Dolenko, P. E. Hänninen, D. I. Vlasov, V. G. Ralchenko, S. Hosomi, I. I. Vlasov, C. Sahlgren, J. M. Rosenholm, *Nanoscale*, 2013, **5**, 3713-3722.
49 C.L. Tseng, I.L. Shih, L. Stobinski, F.H. Lin, *Biomatreials*, 2010, **31,** 5427-5435.
50 L. Faucher, A.A. Guay-Begin, J. Lagueux, M.F. Cote, E. Petititclerc, M.A. Fortin, *Contrast Media & Molecular Imaging*, 2010, **6**, 209-218.
51 Y.-S. Lin, Y. Hung, J.-K. Su, R. Lee, C. Chang, M.-L. Lin, C.-Y. Mou, The Journal of Physical Chemistry B. 2004, **108,** 15608-15611.
52 A. Y. Stakheev, E. S. Shpiro, J. Apijok, *The Journal of Physical Chemistry*, 1993, **97**, 5668-5672.
53 Y. Kobayashi, H. Morimoto, T. Nakagawa, Y. Kubota, K. Gonda, N. Ohuchi, *Journal of Nanostructure in Chemistry*, 2013, **3.**
54 X.-H. Long, P.-Y. Yang, Q. Liu, J. Yao, Y.Wang, G.-H. He, G.-Y. Hong, J.-Z. Ni, *BioMetals*, 2011, **24**, 663-677.
55 H. Ersoy, F. J Rybicki, *Journal of Magnetic Resonance Imagin*g, 2007, **26**, 1190-1197.
56 S.Aime, P. Caravan, *Journal of Magnetic Resonance Imagin*g, 2009, **30**, 1259-1267.
57 S. Aime, A. Barge, C. Cabella, S. Crich, E. Gianolio, Current Pharmaceutical Biotechnology, 2004, **5**, 509-518.